
Article:

Carr, A.S., Bateman, M.D., Cawthra, H.C. et al. (2019) First evidence for onshore marine isotope stage 3 aeolianite formation on the southern Cape coastline of South Africa. Marine Geology, 407. pp. 1-15. ISSN: 0025-3227

https://doi.org/10.1016/j.margeo.2018.10.003

First evidence for onshore Marine Isotope Stage 3 aeolianite formation on the southern Cape coastline of South Africa.

Andrew S Carr[1*], Mark D. Bateman[2], Hayley C Cawthra[3,4], Judith Sealy[5]

1: School of Geography, Geology and the Environment, University of Leicester, University Road, Leicester LE1, 7RH

2: Department of Geography, University of Sheffield, Winter Street, Sheffield S10 2TN, UK

3: Council of Geoscience, PO Box 572, Bellville 7535, South Africa

4: African Centre for Coastal Palaeoscience, Nelson Mandela University

5: Department of Archaeology, University of Cape Town, Private Bag X3, Rondebosch, 7701, Cape Town, South Africa

*corresponding author: asc18@le.ac.uk tel +44 (0)116 2523851

Abstract

The southern Cape coast of South Africa boasts an impressive suite of Plio-Pleistocene aeolian dune deposits (aeolianite). Previous research has shown that in this region onshore dune accumulation was generally focused around interglacial sea level highstands, with the locus of coastal dune accumulation shifting onto the adjacent continental shelf during glacial sea level lowstands. Here, using new luminescence dating results, we present the first evidence for preserved *onshore* glacial age dunes. Specifically, on the Robberg Peninsula, a rocky headland 28 km east of Knysna, two phases of aeolianite formation are identified, corresponding to early (45-60 ka) and late (35-30 ka) marine isotope stage (MIS) 3. Subsequently, during the Holocene, all substantive dune accumulation occurred between 10.2 and 7.0 ka, forming cliff-fronting dunes and filling the limited accommodation space on the headland, including an archaeological rock-shelter. Combining these ages with bathymetric data, we infer that this distinct onshore glacial age aeolianite record reflects: 1) restricted accommodation space during sea level highstands; 2) a regional narrowing of the continental shelf, and 3) liberation of sediments lying on a prominent -45 to -60 m offshore terrace, which would have been exposed during MIS 3. This demonstrates that despite broad regional-scale trends in the timing of coastal aeolian activity - driven by commonalities in relative sea level trends and climate - distinct local variations in late Quaternary coastal evolution can be identified. This is ascribed to local controls on preservation (accommodation space) and sediment supply (shoreline position and antecedent offshore sediment supplies). Such findings may have wider implications for interpretations of site context/resource availability at several notable coastal archaeological sites, and more broadly suggest that local offshore or onshore geologic contexts can at times assume greater influence on a preserved coastal aeolianite record than the regional-scale trends in sea level and climate.

Keywords: coastal dune, sea level, luminescence dating, Holocene, Pleistocene, archaeology

1. Introduction

The passive margin southern Cape coast of South Africa (**Figure 1**) preserves an impressive record of Plio-Pleistocene sea-level change and associated coastal dune formation. The latter comprises extensive suites of carbonate-cemented aeolian dunes ("aeolianite") (Roberts et al., 2011; 2013). Coastal aeolianites are typically associated with temperate carbonate shelves (Brooke, 2001) and, considered globally, the southern Cape aeolianites are particularly extensive and well-studied, with some of the largest examples preserved as the ~200 m high barriers of the Wilderness Embayment (Martin, 1962; Tinley, 1985; Illenberger, 1996; Bateman et al., 2011; **Figure 1**). Aeolianites are widespread from Cape Town (Roberts et al., 2009) to Port Elizabeth and are formally mapped as the Cenozoic Bredasdorp Group (Malan, 1989). They tend to young in a seaward direction (Roberts et al., 2008), with deposits near the contemporary coastline largely dating from the middle Pleistocene to the Holocene (Roberts et al., 2008; 2013). The widespread application of optically stimulated luminescence (OSL) dating has created a relatively detailed picture of the links between the sea-level change and past episodes of onshore coastal dune/aeolianite accretion (Bateman et al., 2004; Carr et al., 2007; Roberts et al., 2008; Bateman et al., 2011; Roberts et al., 2012; 2013; Cawthra et al., 2012; 2014; 2018). There are now more than 100 published OSL ages for southern Cape aeolianites. The resulting emplacement timings and dune types are inferred to broadly reflect the interplay between sediment supply (mediated by relative sea-level change), underlying geological/topographic controls, which determine shoreline positions through time (Bateman et al., 2011), and climatic controls (via vegetation cover) on the propensity for dunes to migrate inland or be stacked vertically (Roberts et al., 2009). The coastline is considered to have experienced limited tectonic activity (and associated vertical motion) during the middle-late Pleistocene (Roberts et al., 2012).

Most phases of dune/aeolianite formation preserved onshore are associated with relatively high sea levels prior to, during and immediately after interglacial sea level highstands, particularly marine oxygen isotope stages (MIS) 11, 7, 5e, 5c and 5a (Bateman et al., 2004; Roberts et al., 2008; 2012; Carr et al., 2010; Bateman et al., 2011). The need for a proximal shoreline sediment source is implied and indeed amino acid racemisation analyses have further demonstrated the importance of nearshore sediment reworking during highstands for the construction of barrier dune systems (Roberts et al., 2008). On the southern Cape, sea levels repeatedly attained similar elevations which, combined with a relatively humid climate, promoted the vertical accretion of coastal dune systems, as opposed to extensive inland migration (Illenberger, 1996; Roberts et al., 2009). This limited landward migration of dunes is thought to account for an absence of onshore dune ages from glacial periods (i.e. MIS 4-2), when the sediment source, and thus locus of net dune accumulation, tracked southwards onto the continental shelf (Birch et al., 1978; Martin and Flemming, 1986; Cawthra et al., 2012; 2014; 2018).

Somewhat different coastal dune/aeolianite records are seen elsewhere. On the KwaZulu-Natal coastline (South Africa), for example, last interglacial coastal dune systems were both weathered (de-calcified) and in places reworked during MIS 2 (Botha et al., 2003; Porat and Botha, 2008). Further afield, and in contrast to South Africa, aeolian reworking of exposed continental shelf sediments has been invoked to account for MIS 3 aeolianite formation in Western Australia (Brooke et al., 2014; 2017). Similarly, drier glacial climates and exposed continental shelf sediments during lowstands are inferred to account for MIS 5c/b, 4 and 3 aeolianite formation in the Mediterranean basin (Fornos et al., 2009; Andreucci et al., 2012). On the southern Cape of South Africa offshore dunes have been mapped (Bateman et al., 2011, Cawthra et al., 2012; 2014) and have recently been shown to date to ~110 ka and 80 ka (Cawthra et al., 2018), but thus far no onshore MIS 3 or MIS 2 aeolianite has been identified.

In this study, we present new bathymetry and lithological data, and a suite of new OSL ages for aeolianites and dunes located in an unusual southern Cape context: the prominent headland of the Robberg Peninsula, south of Plettenberg Bay (**Figures 1 and 2**).

In rocky coast contexts, cliff-fronting and climbing-dune aeolianites have been described in detail in the Mediterranean Basin (Clemmensen et al., 1997; Fornos et al., 2009; Andreucci et al., 2010a; de Valle et al., 2016). In such situations, where there is much more restricted onshore accommodation space, it has been shown that there is a strong dependency on relative sea-level change to promote periods of dune accumulation, via liberation of a sediment source and provision of new accommodation space for dunes to form within. By contrast, in South Africa, few studies have considered aeolianite from headlands although several locales, such as Pinnacle Point (near Mossel Bay), show evidence that some contemporary rocky headlands did, at times, host sandy beach-dune systems that are no longer present (cf. Shaw et al., 2001; Bateman et al., 2004; Jacobs, 2010). The Robberg Peninsula therefore presents an important opportunity to consider a variant of the broad southern Cape glacial-interglacial coastal geomorphic response. In this context, the aims of this study were to:

- use OSL dating to provide a suite of numerical age constraints for southern Cape aeolianites/dunes in a headland rocky-shoreline setting;
- consider the timing of dune activity in light of newly digitised offshore single-beam bathymetric data and existing literature pertaining to offshore sediment composition;
- consider the drivers of dune formation/preservation in high-energy, headland environments of the southern Cape;
- relate these findings to the regional patterns of aeolianite deposition in South Africa and further afield.

2. Study area

2.1 Geomorphic setting and the Robberg Peninsula

Structurally the southern Cape coastline comprises three key elements - the Cape Fold Belt mountains, an (onshore) seaward-dipping coastal platform and a broad continental shelf (Birch, 1978) (**Figure 1**). The Cape Fold Belt is the result of orogenesis of the Cape Supergroup ~278 – 230 Ma (Newton et al., 2006). Following fragmentation of Gondwana and the opening of the South Atlantic in the Early Cretaceous (~136 Ma) (Martin and Hartnady, 1986), offshore, arcuate normal faults bounded several graben and halfgraben structures, which became depocentres for Mesozoic and Cenozoic terrigenous sediments (Tinker et al., 2008 a,b). The half-grabens morphologically manifest themselves as a series of rocky headlands separated by embayments. The latter particularly occur where Bokkeveld Group shales have been preferentially eroded (e.g. Roberts et al., 2013). These basins contain Late Mesozoic clastic sedimentary infills (e.g. Enon and Kirkwood Formations) and have tended to be loci for Neogene - Quaternary aeolian and marginal-marine deposition (Roberts et al., 2008; Marker and Holmes, 2010). This structural control defines the major aeolianite-containing embayments (e.g. Still Bay and Mossel Bay). The Wilderness Embayment is an exception, in that the embayment is the result of preferential erosion of less resistant Precambrian strata (Dunajko and Bateman, 2010), but it too presents a significant space within which barrier dunes and back-barrier lagoons have formed and been protected from subsequent erosion during the last 250,000 years (Bateman et al., 2011).

Plettenberg Bay, approximately 50 km east of Wilderness, is one of a series of eastward-opening headland bays of the southern Cape (**Figure 1**). It has a log-spiral planimetric shape (Bremner, 1983) and has developed in the lee of the Robberg Peninsula, which defines its southern boundary. Plettenberg Bay lies at the eastern margin of the Agulhas Bank, at the divide between the broad shelf to the west and a narrower shelf to the east (**Figure 1**). The shelf break at Robberg occurs at about 200 m water depth, which is ~90 km to the south. The -100 m isobath, however, is only 19 km from the coast. The Robberg Peninsula extends 3.7 km into the Indian Ocean (**Figures 1 and 2**). It is orientated E-W (aligned on a heading of 106°) and is the only true peninsula on the entire southern Cape coastline. It varies in width from 0.75 km to 0.2 km (the latter represents "The Gap"- a narrowing at the western end of the peninsula) and reaches 120 m above sea level at its eastern end. Geologically, it comprises quarzitic sandstones of the Early Cretaceous Robberg Formation and younger Cretaceous conglomerates (Toerien, 1979; Reddering, 2003). The Robberg Formation consists of sandstone, subordinate conglomerate and breccia, reaching a thickness of 95 m (Reddering, 2003). The overlying Enon Formation comprises reddish-brown to orange-yellow conglomerate with infrequent interbedded sandstone and mudstone (Shone, 2006). Clasts were derived from the arenaceous Table Mountain Group north of the Gamtoos Basin. The shoreline around much of the peninsula is rocky, with well-developed shore platforms at the southeast end of the peninsula (**Figure 2**). Three rivers, the Piesang, Bitou and Keurbooms enter Plettenberg Bay, with the latter two sharing a combined estuary mouth at Formosa Bay. The estuaries act as sediment traps and allow only the fine fraction of sediment to pass through in suspension during floods (Reddering, 1983).

The Peninsula presently features an active "headland-bypass" dune system (*sensu* Tinley, 1986; Illenberger and Burkinshaw, 2008) which comprises a climbing-falling dune system ("Witsand") located mid-way along the Peninsula (**Figure 2)**. This produces net cross-headland sand transport, which is a significant component of the down-drift/down-wind Robberg Beach sediment budget (Hellström and Lubke, 1996). The source of sand is a large tombolo formed between "The Island" (an offshore aeolianite stack; Butzer and Helgren, 1972) and the peninsula (**Figure 2**). The tombolo is a similarly unique feature on the southern Cape. South of "The Gap" on the steep coastal cliffs of the southwestern peninsula, several archaeologically-significant caves have formed, notably Nelson Bay Cave (Klein, 1972; Deacon, 1984; Inskeep, 1987) and Hoffman's Cave (also known as East Guanogat Cave; Butzer and Helgren, 1972; Rudner and Rudner, 1973; Kyriacou, 2009). Immediately east of Hoffman's Cave the first significant accumulations of uncemented aeolian sands occur, comprising well-vegetated unconsolidated dune sands banked against the rock cliff-line west of the tombolo (**Figure 2**). Moving eastwards to the tip of the peninsula, the unconsolidated dune sand cover is much thinner, but significant exposures of well-cemented aeolianite are found along the southeast margin of the peninsula.

2.2 Climate and oceanography

The Plettenberg Bay area is part of the year-round (aseasonal) rainfall zone that characterises the southern Cape coast between George and Port Elizabeth. This region represents the transition between the winter rainfall zone of the west and the summer rainfall zone to the east. Thus, the area is relatively humid and mean annual rainfall is in the range of 800-1000 mm yr^{-1}. To the south and east of Robberg, the near coastal current flow is in a westerly direction (Tripp, 1967) in response to the Agulhas counter-current and flows at an average rate of 1.5 knots. On the southern Cape coast, the prevailing winds are from the west to west-southwest, with a strong easterly and east-southeasterly component during the spring and summer months. The strongest wind speeds (which may exceed 20 m s^{-1}) occur in the austral winter/spring between July and October (Hellström and Lubke, 1996), coincident with the passage of westerly systems through the Cape winter rainfall zone. The dominant wave regime is from the southwest (Silvester, 1974; Bremner, 1983) and the long-period waves are diffracted around the Robberg Peninsula. Median significant swell heights in this region (east of Knysna) are of the order ~2.5 m and the spring tide range is approximately 2 m (Whitfield et al., 1983). The coastline is thus considered microtidal (e.g. Cooper, 2001).

3. Sampling sites

We aimed to describe and provide age constraints for the major occurrences of aeolian sediments on the Robberg Peninsula. These comprise: 1) the aeolianites on the southeastern margin of the Peninsula; 2) aeolianites on the offshore stack ("The Island") south of the Peninsula; 3) unconsolidated, but vegetated dune sands west of the active Witsand system and 4) a thick sequence of aeolian sand preserved *within* Hoffman's Cave, west of Witsand.

3.1 The Robberg Peninsula

Aeolianite is exposed for ~800 m (laterally) near the Peninsula tip (**Figure 3**). At the eastern-most exposure (sample Leic13004) aeolianite is preserved in a distinct topographic low in the underlying Robberg Formation. The aeolianite presents high-angled foreset beds (measured dips ranging between 28 and 32°) dipping to the ENE (measured range 68-90°) and is well-cemented, with limited evidence of root bioturbation or rhizoliths. Small-scale slump structures are apparent in some locations. About 400 m to the west, additional semi-continuous (alongshore) exposures of well-cemented aeolianite are seen. The upper surface of the aeolianite here is characterised by abundant rhizoliths, and close to OSL sample Shfd13049 (Figure 2) it is overlain by a veneer of ~1.5 m of uncemented dune sands. The aeolianite is characterised by high-angle (28-30°) foreset beds dipping in easterly or north-easterly directions (measured azimuths 80-100°). At the western limit of these exposures, (sample Leic13005), similarly well-cemented aeolianite is preserved within a low point in the underlying Robberg Formation (**Figure 3**). At present, it is also protected from marine erosion by large hard-rock outcrops and boulders, and an extensive shore platform.

3.2 The Island

A striking feature of the study area is “The Island”; an aeolianite stack connected to the peninsula by a 300 x 500 m sandy tombolo (**Figures 2, 4 and 5a/c**). The tombolo Island length (I) to offshore distance (J) ratio is ~1.6 and is typical of tombolo forms in high-energy settings (Sanderson and Elliot, 1996). The Island itself measures ~450 m x ~150 m with a long axis orientation of 73°. It is composed entirely of aeolianite, with an upper veneer of uncemented dune sands. (**Figure 4**). Butzer and Helgren (1972) provided a detailed description of The Island’s stratigraphy (although not of aeolianite elsewhere on the Peninsula) and argued that it is a remnant of a former barrier dune system (identifying topsets and backsets and foreset bedding structures). They described two well-developed palaeosols (P1 and P2) separated by ~8 m of aeolianite. A radiocarbon date of 7300 ± 120 ^{14}C yr BP (UW201: 7595-8015 cal yr. BP; **Table S1**) was obtained from a terrestrial gastropod (*Achatina zebra*) in uncemented dune sands stratigraphically above the upper Palaeosol P2. A second radiocarbon date of 16,000 ± 220 ^{14}C yr BP (18,770-19,800 cal yr. BP; **Table S1**) from the lower palaeosol (P1) was obtained using “inorganic carbonate” and is of questionable reliability. The total thickness of the aeolianite below P1 was estimated to be > 30 m (Butzer and Helgren, 1972).

The two major palaeosols are readily apparent, although subtler protosols and weakly decalcified layers can be identified within the aeolianite (i.e. between P1 and P2) on the northwestern side of The Island. The upper palaeosol P2 is a prominent feature running across much of the upper surface (**Figure 4**). It comprises de-calcified/rubified sands, underlain by an often well-developed calcrete, comprising both nodular and massive (hardpan) pedogenic calcrete types. It is overlain by up to 2 m of unconsolidated sands containing abundant terrestrial gastropods (presumably the same sands/shells from which Butzer and Helgren’s (1972) radiocarbon date was obtained). At the northwest edge of The Island a large shell midden dominated by *Perna perna* (Mytilidae) and containing Later Stone Age (LSA) artefacts is preserved, the base of which dates to 2870-3116 cal yr. BP (**Table S1**). Unconsolidated sands immediately underlying the midden, but overlying palaeosol 2 were sampled for OSL dating (Leic13002). Beneath these sands P2 is clearly expressed and is, in turn, underlain by rhizolith-rich aeolianite (relating to OSL sample Shfd13047, sampled below the rhizolith horizon). At the southwestern (seaward facing) margin of The Island landwards-dipping (~20°) aeolianite (OSL sample Shfd13048) is exposed. This lies stratigraphically between P1 and P2, while on the southern side of The Island the two palaeosols are separated by 9.5 m of well-cemented aeolianite (OSL sample Leic13003). As on the mainland, the aeolianite is characterised by high-angle eastwards dipping beds. The upper layers are root bioturbated, but two prominent foreset units are also separated by a unit of low-angle laminated beds (see also Butzer and Helgren, 1972), which are exposed on the SE side of The Island (also between P1 and P2).

3.3 Unconsolidated dunes in the Witsand system and Hoffman's Cave

Beyond the Witsand system, unconsolidated and/or vegetated dune sands are limited in occurrence. However, significant dune deposits are found ~300 m west of Witsand, forming a distinct cliff-front dune reaching ~31 m above the shoreline (**Figure 5b**). The crest line of the dune runs for 150 m alongshore and is ~10-20 m in front of the hard-rock cliff line. The distance between the dune crest and cliff narrows to the NW as the cliff line lowers and this feature is interpreted as an echo dune (Clemmensen et al. 1997). Augering from the dune brink revealed a total sand depth of 10.5 m. Four samples (Leic13008, Leic13007, Shfd13052 and Shfd13053) were obtained for OSL dating. Hoffman's Cave lies a further 100 m west of the echo dune. This contains ~1.6 m of LSA shell midden deposits (**Figure S1**). There have been several attempts to provide a chronology for this deposit (Butzer and Helgren, 1972; Fairhall et al., 1976). The best resolved dates were obtained on charcoal from a controlled excavation in 2007-2008, and range from 3453-3644 cal. yr BP (Beta-241142) to 4233-4529 cal yr. BP (Beta-241146) (Kyriacou, 2009; **Table S1**) Beneath the LSA deposits several metres of archaeologically-sterile dune sand were reported in previous excavations, the basal depth and age of which (along with the presence of any underlying archaeology) were unknown. Here, through augering we sampled these sands for OSL dating to a depth of 5.5 m (See **Figure S1** for details of the specific stratigraphic relationships).

4. Methods

4.1 Offshore bathymetry

A new bathymetric map, used as a basis for offshore interpretations, was constructed through a compilation of existing datasets (SANHO, 1972; Flemming et al., 1983) and gridded at the Council for Geoscience using the statistical method of Kriging in software *Surfer 9* to smooth the varying resolutions. Additional datasets were derived from single-beam echo-sounding data collected by the Fisheries Division of the Department of Agriculture, Forestry and Fisheries during routine demersal cruises on the vessels R/V Africana and R/V Algoa (de Wet, 2013) and satellite altimetry data from the ETOPO1 - 1Arc-Minute Global Relief Model (Amante and Eakins, 2009).

4.2 Sediment Characterisation

Particle size distributions (0.01-3500 µm) for dune sands and aeolianites were obtained using a Mastersizer 3000 laser particle size analyser (Malvern Panalytical Ltd.), following treatment with dispersant. To consider geochemistry, metal oxide concentrations were determined via XRF (PANalytical Axios Advanced XRF spectrometer) at the University of Leicester with additional trace element data (some of which was used for environmental dose rate measurements for OSL dating) determined via Inductively-Coupled Plasma-Mass Spectrometry (ICP-MS) using a ThermoScientific ICAP-Qc quadrupole ICP mass spectrometer. For this, samples were dissolved in a metal acid mixture (HF, HCl, HNO_3) at 120°C in sealed containers for 12 hours.

4.3 OSL dating

Fifteen OSL samples were obtained from natural exposures by hammering opaque steel / plastic tubes into exposed sediment, or by cutting large blocks of well-cemented aeolianite (Leic13004). The latter was spray painted and broken open under red light conditions. Tube ends were retained for moisture content and dose rate estimates. The echo dune and sands from Hoffman's Cave were obtained using a Dormer sand drill system. Samples were independently prepared and equivalent doses independently measured in the Sheffield University and the University of Leicester OSL laboratories using otherwise identical procedures. Samples were treated with hydrochloric acid to remove carbonates, 32% H_2O_2 to remove organic matter and then sieved to fractions between 250 and 90 µm. Heavy liquid was used to isolate the fraction between 2.58-2.70 g cm^{-3} and the samples were etched in 48% HF for 45 minutes. All measurements were carried out on a Risø TL-DA 20 TL/OSL readers. Sub-samples were mounted as 9 or 2 mm spots on stainless steel disks using silicone spray. The total number of 180-212 µm grains within the area of a 2-mm spot is 150-250 grains.

OSL was detected with an EMI 9235QA photomultiplier tube and a U-340 filter. Stimulation (40 s at 125°C) was provided by blue LEDs (stimulation wave length 470 nm). Laboratory irradiations were produced by a ^{90}Sr beta source, calibrated for using the Risø calibration quartz. Equivalent doses were determined using the single aliquot regeneration (SAR) protocol (Murray and Wintle, 2000; 2003). Dose response curves (DRCs), comprising both zero and recycling dose points were constructed using the first 0.8 seconds of the OSL signal with a background subtraction based on the last 2 seconds. These dose response curves were fitted with saturating exponential fits. Equivalent dose uncertainties include counting statistics, curve fitting uncertainties and a 1.5% systematic uncertainty. Aliquots were rejected from the analysis if they exhibited recycling ratios more than 10% from unity, D_0 estimates (the parameter describing the degree of saturation for a saturating exponential fit) > twice (given measurement uncertainties) the equivalent dose (e.g. Thomsen et al., 2016), recuperation (zero dose signal) >5% of the natural sensitivity-corrected luminescence signal or failed the IR depletion test for feldspar contamination (Duller, 2003). The suitability of the SAR protocol and specific preheating conditions were determined via dose recovery preheat plateau tests (**Table S2**). These demonstrated that accurate and precise determinations of the administered dose could be obtained across a range of preheating conditions. Final equivalent doses (**Table 1**) were derived using the Central Age Model (CAM) of Galbraith et al., (1999) and include an additional 3% laboratory beta source calibration uncertainty within the quoted 1 sigma D_e uncertainties.

Given the sampling of well-cemented aeolian deposits, inter-aliquot equivalent dose scatter due to incomplete bleaching or post-depositional bioturbation was not anticipated to be significant. However, some inter-grain equivalent dose variability has been reported for aeolianites both in this region (Bateman et al., 2004) and beyond (Brooke et al., 2014). As such, supplementary analyses using 2 mm aliquots, and some single grain analyses (**Table 1**) were undertaken. Single grain measurements were conducted using a focused 532 nm Nd:YVO_4 solid state diode-pumped laser emitting at 532 nm focused to a spot ~20 µm in diameter with grains rejected if the test dose signal was less than 3 sigma above background, the relative test dose uncertainty was larger than 20%, or recycling ratio exceeded 20% of unity. Equivalent doses determined via the single grain, 2 mm single aliquot and 9 mm single aliquot analyses are consistent (**Table 1; Figure S2**) and do not suggest the presence of significant numbers of grains with poor OSL properties (which are removed from single grain analyses) that might bias the single aliquot data (e.g. Brooke et al., 2014). The level of over-dispersion for single aliquot and single grain measurements is typical of well-bleached aeolian sediments in this region (Jacobs et al., 2003a; 2003b). Ages obtained using the

Central Age Model (CAM) equivalent dose are thus considered suitable estimates of the burial doses received by the samples.

Environmental dose rates were calculated in an identical manner for all samples (regardless of the laboratory in which the D_e was measured) and were determined using *in-situ* gamma spectrometry (using the "windows" method; Aitken, 1985) or using a combination of ICP-MS analysis and XRF (latter for K_2O content). Elemental concentrations were converted to dose rates following Guerin et al., (2011) and were then corrected for grain size (Mejdahl, 1979), etching (Bell, 1979) and water content (Aitken, 1985). An internal alpha dose rate of 30 ± 8 mGy a^{-1} was included (Jacobs et al., 2003a). Water contents were based on modern values with a 3% (absolute content) uncertainty. The cosmic dose was calculated following Prescott and Hutton (1994) using the measured burial depths. For the Hoffman's Cave samples, the cosmic dose was further adjusted for the shielding of 50% of the horizon by the rock forming the cave.

It was noted, as found elsewhere along the southern Cape, that the elemental ratio of U:Th is relatively high (**Figure 7**, **Table S4**). This most likely reflects the incorporation of marine carbonate (Bateman et al., 2008) and here the highest U:Th ratios are associated with the highest carbonate contents (mostly the aeolianites rather than dune sands). In previous studies in the region, dose rates (and thus OSL ages) derived from such materials have shown acceptable correspondence with independent age control (Bateman et al., 2008; Bar-Matthews et al., 2010). For samples with both gamma spectrometry measurements and ICP-MS measurements (Leic13002, Leic13006) the dose rates (and resulting ages) are in broad agreement (**Table S3**), despite each method measuring differing parts of the ^{238}U and ^{232}Th decay chains. For Hoffman's Cave, independent age constraints are provided by the radiocarbon ages from the overlying LSA deposit. The resulting ages therefore assume no change in burial dose rate.

5. Results

5.1 Offshore topography/bathymetry

The offshore topography is characterised by a distinct terrace with minimum depth of -45 m and a maximum depth of -60 m (**Figures 1 and 6**). This is located close to the contemporary coast and it serves as a platform for the accumulation of shelf sediments between the subaerially exposed peninsula and the steeper offshore shelf below -65 m. Offshore sediments in this region tend to be trapped in the nearshore zone, and at Robberg they form an elongated sediment prism from -45 m, which extends 2 km offshore (see also Martin and Flemming, 1986). Further south, a clear change in gradient between the inner- and mid-shelf is observed as the seafloor drops relatively rapidly to ~-60 to-80 m at ~7 km from the coast. The bathymetry then deepens more gradually to -120 m at the shelf edge, where the MIS 2 Last Glacial Maximum shoreline would have been located, approximately 30 km from the contemporary coastline. The most prominent feature on bathymetric datasets from Robberg is a submerged spit-bar extending south and east of the Peninsula, which rises from -90 m in the south and from -55 m in the north, reaching up to -40 m below Mean Sea Level. This 7.5 km long deposit reaches a maximum thickness of 51 m (average of 40 m). By contrast, the sediments in Plettenberg Bay to the north and further east present a far thinner veneer, reaching a maximum thickness of just 5 m (Birch, 1978).

5.2 Aeolianite/Dune sedimentology and geochemistry

Particle size data for the dune and aeolianite samples are shown in **Table 2**. The aeolianites comprise negatively skewed (-0.20 to -0.06), well-sorted (0.99 -0.63 phi) medium-grained sands (median 1.48 to 1.87 phi). The echo dune and the Hoffman's Cave dune sands are texturally identical to one another, but are finer (median 1.86 to 2.02 phi), better sorted (0.41-0.44 phi), and less-skewed (0.00 to -0.02) than the aeolianites.

In terms of their trace element geochemistry, elemental ratios usually associated with immobile (e.g. zircon) minerals (e.g. Zr/Hf, La(N)/Yb(N)) show no substantial difference between the unconsolidated dunes and aeolianite (although note that the sample numbers are small), suggesting no major differences in their non-carbonate sediment provenance. These ratios are broadly comparable to the Wilderness dune sands (though they appear more variable at Robberg) (**Figure 7;** see also Dunajko and Bateman 2010), with the ratio from the Rare Earth Elements (La(N)/Yb(N)) slightly higher at Robberg compared to Wilderness. The average Ti/Zr ratios for the cemented (0.92) and unconsolidated dunes (0.90) at Robberg are also essentially identical. The total calcium content (largely from $CaCO_3$) and the associated element strontium is distinctly lower in the Robberg unconsolidated dunes compared to the Robberg aeolianite (**Table S4**), although the Sr/Ca ratio is identical (0.005) across the sites, and identical to dunes at Wilderness, reflecting a dominantly foraminifer/coccolith contribution to the carbonate fraction (Kim et al., 1999). The reduced Ca and Sr content of the unconsolidated dunes compared to the aeolianite is mirrored by the trends in several element ratios *viz*: Rb/Sr and Ba/sr (also Th/U) (**Figure 7; Table S4**).

5.3 OSL dating results

All samples produced bright, rapidly decaying luminescence signals (reaching <10% of initial signal within 0.5 seconds), suggesting a dominant quartz fast component OSL signal (**Figure 8**). Consistent with this, dose recovery data (Murray and Wintle, 2003) for a suite of samples demonstrate good accuracy and precision across a range of temperature treatments (**Table S2**). For the Pleistocene aeolianites, equivalent doses fall in the range of 58 to 80 Gy and most aliquots produced equivalent doses below twice the D_0 parameter (for Leic13003 this accounted for 4 aliquot rejections). Very few aliquots were rejected due to failure of recycling ratio, recuperation or feldspar depletion tests (**Table 1**). The independently obtained equivalent doses from the two different luminescence laboratories show good stratigraphic conformity with, for example, Leic13006 producing an age of 7.0 ± 0.3 ka and the subjacent sample Shfd13050 producing an age of 8.7 ± 0.4 ka.

OSL ages for the Robberg Peninsula span 67 ± 4 ka to 7.1 ± 0.4 ka and show clear spatial patterning. The oldest ages are from the aeolianites at the southeast tip of the Peninsula, 67-56 ka (Leic13004, Shfd13049, Leic13005). By contrast, all the sampled aeolianite from The Island (**Figure 9**; samples Leic13001, Shfd13047, Shfd13048, Leic13003), which lies stratigraphically between P1 (lower) and P2 (upper), falls between 35 ± 3 and 42 ± 3 ka. The age of the (inaccessible) aeolianite below P1 remains unknown but may correspond in age with the older aeolianite from the eastern Peninsula. Leic13002 from above P2 (**Figure 4**) produced an age of 6.9 ± 0.4 ka, which is close to Butzer and Helgren's (1972) reported radiocarbon age (dune snail calibrated age of 7595-8105 cal yr. BP) from sands overlying P2, noting that: a) the death of their sampled snail may predate the deposition of the dune sands and b) their exact sampling location is unknown.

The dune sands spanning the depth range of the echo dune east of Hoffman's Cave and underlying the LSA midden in Hoffman's Cave all have early Holocene ages (**Table 1**). For the echo dune, accumulation began at 10.2 ± 0.5 ka (basal sample at 9.8 m depth and 0.5 m above bedrock) and continued to 7.1 ± 0.4 ka (3.3 m depth), with the uppermost two samples producing ages with overlapping uncertainties. The most surficial sample, Leic13008, shows the greatest single grain (and single aliquot) over-dispersion (32% OD; Table 1), reflecting the presence of a small number of higher dose grains (**Figure S2**). No obvious evidence for a depositional break was observed in the sediment during excavation, but it cannot be fully assessed whether there was continuous accumulation between Shfd13052 (8.8 m depth and 9.1 ± 0.4 ka) and Leic13007 (7.1 ± 0.4 ka). The dune sands within Hoffman's cave 150 m to the west closely match the ages of the adjacent dune (9.3 ± 0. ka to 7.0 ± 0.4 ka; **Table 1**) and are also stratigraphically consistent with the age of the overlying LSA midden (**Table S1; Figure S1**). Both sites suggest that the early Holocene was a time of significant aeolian activity on the southern margin of the peninsula.

6. Discussion

The history of onshore dune/aeolianite formation along the southern Cape has been considered in detail, particularly in the Wilderness embayment (Bateman et al., 2004; 2011; Cawthra et al., 2014). Combining findings from studies further west at Mossel Bay (Jacobs, 2010), Still Bay (Roberts et al., 2008; Bateman et al., 2008), the Agulhas Plain (Carr et al., 2006; Bateman et al., 2008) and False Bay (Roberts et al., 2009), there are broadly-comparable trends in the timing of onshore aeolianite/dune emplacement, with accumulation largely associated with interglacial highstands (summarised in Roberts et al., 2013). At the Wilderness embayment, except for two samples of surficial (*decalcified*) sands from the seaward barrier (Carr et al., 2007) there is an absence of OSL ages from the MIS 4 (79 ± 9 ka; Shfd08189) until MIS 1 (6.9 ± 0.4 ka; Shfd04275) (Bateman et al., 2011; **Figure 10**). Based on eustatic sea level trends, at Wilderness this was coincident with a sea level regression to below ~-30 m at c. 80 ka (**Figure 10**), which would have placed the contemporary shoreline ~15 km south of the modern shore (Bateman et al., 2011). The presence of offshore aeolianite ridges demonstrates that coastal aeolian activity tracked the receding shoreline at both Wilderness and Mossel Bay (Cawthra et al., 2014; 2015; 2018). By contrast, the aeolianites at Robberg fall almost entirely within MIS 3 (57-29 ka; Lisiecki and Raymo, 2005), while the unconsolidated dune ages all coincide with the post-glacial Marine Transgression (PMT). The aeolianites therefore represent the first identified onshore MIS 3 aeolianite on the southern Cape. The ages from the southeast Robberg Peninsula correspond to early MIS 3, while the ages from upper strata of The Island cluster towards the end of MIS 3 (36-42 ka). Plotted in relation to the Wilderness dataset (**Figure 10)** they fill a significant and longstanding gap in our coastal geomorphic-aeolian record. These new ages present several questions: 1) why are MIS 5 aeolianites absent at Robberg despite extensive MIS 5 accumulation elsewhere? 2) why only in the context of Robberg has onshore evidence of MIS 3 dune activity been preserved? 3) how do these ages/mechanisms relate to the regional pattern of aeolianite deposition?

6.1 Why are there no MIS 5 aeolianites at Robberg?

On the southern Cape, large headlands such as Cape Agulhas, Buffels Bay and Cape St. Francis are associated with substantial accumulations of unconsolidated dunes and aeolianite, which can be traced to coastline/beaches orientated perpendicular to the prevailing (westerly) sand transporting winds (Tinley, 1985; Carr et al., 2006; Claassen, 2014). This has generated extensive headland dune systems, which in some locations connect with the down-drift embayment forming "headland by-pass" dunefields (Illenberger and Burkinshaw, 2008; Roberts et al., 2009). These have been shown to date to both the Holocene (Carr et al., 2006; Bateman et al., 2008) and to previous interglacials (Roberts et al., 2009). The apparent absence of MIS 5 aeolianite at the smaller (and differently orientated) Robberg headland must therefore reflect a lack of accommodation space (**Figures, 2, 3 and 5).**

At Robberg today, except for the small beach at The Gap and the larger tombolo system (which is contingent on the presence of The Island – see below), there are no sandy beaches to supply dune systems, and much of the modern shore is characterised by shore platforms backed by cliffs cut into the pre-Quaternary sandstone (**Figure 2**). This was probably the case during MIS 5e when the site was also likely to have been a peninsula and, as today, would have been a focus for incoming swell wave energy (e.g. Heydorn and Tinley, 1980). The 6-8 m higher relative sea level during the last interglacial would have further limited the potential for dune accumulation (Carr et al., 2010; Cawthra et al., 2018). The Robberg

MIS 3 aeolianites are likely to have been preferentially preserved because they lie within (and in some cases, are presently protected from the sea by) the underlying hard-rock geology (**Figure 3**). Partial analogues for this situation can be identified. For example, at Pinnacle Point (near Mossel Bay to the west) only vestiges of MIS 5 and older aeolianites are preserved in cliff crevasses and caves (**Figure S3**), with caves covered by dunes at 90 ka (MIS 5c; Jacobs, 2010). By contrast, in low-lying large embayments such as Wilderness, multiple generations of aeolianite dunes could form through MIS 5 and older interglacials and have been preserved. Such a lack of sediment source and/or accommodation space for MIS 5 aeolianite preservation has been cited elsewhere, including in the Mediterranean Basin (Fornos et al. 2009; Andreucci et al., 2010a; 2010b; del Valle et al., 2016).

6.2 Why are there only MIS 3 aeolianites preserved on-shore at Robberg?

To answer this, the interplay between shoreline position, sea level and sediment supply needs to be examined. Comparing the Robberg OSL ages with a eustatic sea level curve for the last glacial cycle (**Figure 10**), we infer that potential for dune/aeolianite formation existed at Robberg only after ~70 ka. Considering the offshore topography around the Peninsula in more detail, the high-resolution profiling results combined with the seismic profiling of Martin and Flemming (1986), Birch (1978) and de Decker (1983) show a -45m to -60 m terrace, with the -60 m isobath located <5 km from the modern shoreline. This terrace separates the inner- and mid-shelf on the south coast and can be identified at Robberg and beyond (**Figures 1 and 6;** Cawthra et al., 2015). Below this, the sea floor gradient is much reduced, such that during MIS 4 and late MIS3/early MIS 2 when sea level lay between -70 and -90 m, the shoreline position, while variable (due to the lower gradient), would have been >7 km from Robberg. We observe most aeolianite ages at Robberg are clustered around the two sea level highstands within MIS 3 (**Figure 10**) at which time sea level would have intersected the relatively steeper terrace between -45 and -60 m

(**Figures 6 and 10**). Sea level fluctuations within this period will have occurred but would not have resulted in substantial lateral movements of the shoreline, maintaining a proximal sediment supply/shoreline. During MIS 2, when sea level fell below -90 m (27 ka to ~14 ka), the shoreline would have receded ~30 km to the south of the modern peninsula, isolating the Robberg dunes from their sediment source.

In terms of sediment sources, this part of the south coast shelf is considered starved of terrestrial sediment inputs. However, approximately 43% of the total bedload sediment of the wider southern Cape shelf is located between Wilderness and Plettenberg Bay (Birch, 1978). The sediments that form the submerged spit-bar off the Robberg Peninsula (**Figure 6**) represent the termination of sediment deposited by this substantial (>11,000 x 10^6 m^3; Birch, 1978) eastward-flowing littoral drift system. Seismic profiling (Birch, 1978) indicates that the spit-bar is composed of two sedimentary units; a lower one composed of reworked muddy sediment, presumably derived from fluvial activity on the shelf during times of lowered sea level, and an upper one formed from sandy material probably derived via redistribution of the aforementioned sediment offshore of Wilderness by eastward longshore littoral drift (e.g. Dingle and Rogers, 1972; Birch, 1978; Cawthra et al., 2015). Texturally, the upper sediments of the spit-bar are comparable to those presently forming the beaches of Plettenberg Bay and are characterised by poorly sorted, polished quartz grains (mean grain size ranging from 2 to 3.5 phi) and shell fragments of a coarser texture (de Decker, 1983).

The major factors controlling sedimentation on the south coast are therefore the effects of transgressive seas on a flat, shallow shelf, a powerful longshore littoral drift system, and coastal aeolian transport (Birch, 1978). The submerged sediment spit-bar likely formed during the postglacial transgression and during the Holocene has built outwards, receiving sediment via the aforementioned littoral drift system. If an analogous deposit formed during MIS 5e and was then exposed by a later sea level regression it would have potentially provided a sandy sediment source for the Robberg Peninsula.

Given the volume of the spit-bar system today, the aeolianite systems at Robberg, formed largely below modern sea level (The Island being a remnant), were potentially extensive features. Indeed, Butzer and Helgren (1972) specifically proposed that The Island is a remnant of a larger barrier dune system. This is difficult to evaluate further, but the prolonged proximity of the shore for much of MIS 3 (driven by the offshore topography) may have been sufficient to create such a feature, given the volume of barrier dune sediments that have demonstrably accumulated during MIS1 at Wilderness. There are remnants of MIS 3 barrier features preserved offshore (Cawthra et al., 2014; 2018) elsewhere on the southern Cape, although perhaps tellingly, as also noted by Martin and Flemming (1986), there are no (presently known) submerged aeolianites immediately west of Robberg. The geochemistry of the Robberg dunes and aeolianite are consistent with this narrative in that: 1) their "immobile" element ratios/compositions are essentially similar to each other and to those of the Wilderness region (see also Dunajko and Bateman, 2010), implying a similar provenance; 2) the Pleistocene aeolianite is more carbonate rich, akin to the upper (modern) spit bar composition and the up-drift aeolianites; 3) the Holocene dunes have lower carbonate contents, which is perhaps evidence for a different offshore sediment source and/or a greater contribution from "pre-weathered" continental shelf sediment, reworked during the PMT, rather than from the spit bar system (**Figure 7**).

In summary, although the regional-scale sediment supply at Robberg is/was essentially the same as Wilderness, the timing of dune/aeolianite formation at Robberg was strongly mediated by onshore accommodation space, sea level change and potentially the formation of a specific local offshore sediment supply. As with cliff-fronting dune systems in the Mediterranean, aeolianite formation here was thus contingent on sea level regressions. This had the combined effect of exposing a supply of (previously unavailable) sediment and provided accommodation space for dunes and/or barrier systems at this (then former) headland. The offshore terrace -45 to -60 m meant that the shoreline position was relatively stable during MIS 3, promoting dune/aeolianite accretion.

6.3 What controlled Holocene dune accumulation?

The echo dune and the aeolian sediments within Hoffman's cave are focused on the early Holocene, coinciding with the post-glacial sea level transgression (**Figure 11**). The earliest age at 10.2 ± 0.4 ka (Shfd13053) corresponds to an RSL of -25 to -45 m (Waelbroeck et al. 2002). In contrast to coastal dune systems from other parts of the southern Cape (e.g. Carr et al., 2006; Bateman et al., 2008; 2011) there are no dune ages post-dating the mid-Holocene relative sea level high stand, which occurred ~7 to 5 ka (Compton, 2001; **Figure 11**). During this time sea level on the south coast were as much as 2.8 m higher than present. This is based on *in-situ Loripes clausus* shells from Knysna dated to 6012-6243 cal yr. BP (Pta5860; 5910 ± 30 ^{14}C yr. BP; **Table S1**) (Marker and Miller 1993) and *Loripes clausus* shells found at +1.7 to +2.7 m in the Keurbooms Estuary dated to 5128-5546 cal yr. BP (Pta4317; 5180 ± 70 ^{14}C yr BP; **Table S1**) (Reddering, 1988). The final stages of dune deposition at both Hoffman's Cave and the adjacent echo dune (7.1 ± 0.4 ka) thus immediately precede this early-mid Holocene relative sea level highstand.

Subsequently, dune activity on Robberg has been limited to the Witsand climbing-falling dune system (Butzer and Helgren, 1972; Hellström and Lubke, 1996). Today, there are no sandy beaches upwind of Hoffman's Cave or the echo dune, (**Figure 2**) implying considerable shoreline re-configuration during the early-mid Holocene, when relative sea level was still rising. The sand of beaches formed at this time was probably sourced from reworked shelf sediments as relative sea level rose. Geochemically, the Holocene dune sands (Hoffman's Cave and the echo dune) contain lower abundances of mobile elements compared to the aeolianites (**Figure 7**); as this difference is not indicative of greater post-depositional weathering (i.e. they are substantially younger features in the landscape), it probably reflects reworking or pre-weathering of sub-aerial continental shelf sediments prior to the PMT. This may also account for the finer and better sorted texture of the Holocene dunes compared to the aeolianites.

When the shore reached levels comparable to or slightly above the present, Robberg would have been established as a prominent Peninsula and the resulting concentration of swell wave energy (Heydorn and Tinley, 1980) removed any sandy beaches, except for the sands of the tombolo, which are protected by (or had begun to accumulate due to) the presence of The Island. The Island is critical to the formation of the tombolo (by definition), inducing swell convergence in its leeside (Sanderson et al., 1996; Sanderson and Elliot, 1996). It is presently asymmetric, presenting a longer shoreline on the west-southwest side, which faces the predominant SW swell (and wind) direction. Once formed, given the orientation relative to the prevailing winds, all subsequent aeolian activity focused on the Witsand system. Mid- to late-Holocene dune activity on Robberg Peninsula was thus characterised by net sediment transfer across the peninsula, presenting a further contrast with embayment dune systems, such as Wilderness, where significant late Holocene (vertical) parabolic dune accretion occurred (Illenberger, 1996; Bateman et al., 2011). Butzer and Helgren (1972) identified buried soil profiles within the Witsand system, implying some variation in either the level of activity, or the locus of active sand movement (See also **Figure 2**). Snail shells within these buried sands were dated to 3837-4246 cal. yr BP, (UW-199; 3740 ± 70 ^{14}C yr. BP; **Table S1**) (Butzer and Helgren, 1972) confirming activity post-dating the early Holocene dune activity in and around Hoffman's Cave. In summary, these rather specific spatial-temporal patterns in Holocene dune formation illustrate the role of sea level stabilisation and the more unusual formation of the tombolo system in controlling the timing and locations of Holocene dune activity.

6.4 How does this relate to the regional patterns of aeolianite deposition?

Direct dating of the Robberg aeolianites to MIS 3, in conjunction with the recent dating of offshore aeolianite (Cawthra et al., 2018) confirms that aeolian activity was, in essence, continuous along the southern Cape coast throughout glacial-interglacial cycles. As the region is considered generally tectonically stable, for both rocky headlands and embayments the primary factors controlling whether onshore dunes were formed and preserved are accommodation space, sea level change and local sediment supply. In embayments where accommodation space is high, the repeated establishment of interglacial high stand coastlines at similar locations led to extensive stacked barrier dunes and high preservation potential. Off-shore preserved, but now submerged dunes formed in front of embayments, but were spread across a large area as the coastline transgressed over low gradient topography (**Figure 1**). Where accommodation space was limited, as on rocky headlands, sea level high stands inevitably led to erosion of pre-existing dunes. At Robberg, however, the presently submerged nearshore terrace provided a coastline of sufficient stability for dune formation during periods in MIS 3 when sea level was lower than present. Here, preservation of the sub-aerial Island outcrop has allowed us to identify this differently aged aeolianite. Additional near-shore seismic analyses might allow the identification of similarly aged and more extensive offshore remnants.

It has been argued that the broad commonalities seen elsewhere in the wider southern Cape onshore aeolianite record reflect comparable trends in relative sea level (including general tectonic stability; Roberts et al., 2012), wind direction (Carr et al., 2006; Roberts et al., 2008) and (in contrast to the west coast) sufficient humidity to ensure that dunes are stabilised relatively close to the shoreline (Roberts et al., 2009). The situation at Robberg illustrates the need to consider both regional and local-scale factors in studies of coastal evolution. Local geological/bathymetric settings are shown to exert a potentially strong secondary impact on the timing and character of preserved coastal dune/aeolianite record. This has been previously observed at several locations in the Mediterranean Basin, such as Mallorca (e.g. Fornos et al., 2009), Ibiza (del Valle et al., 2016) and Sardinia (Andreucci et al., 2010a; 2010b). Such events may be further supported by inherited offshore sand supplies that (in this case) accumulated during the immediately preceding highstand.

7. Conclusions

This study adds to our knowledge of the diversity of local-regional scale coastal aeolian landform responses over glacial-interglacial cycles, and directly illustrates the key role a site's local geological framework has in influencing the timing and preservation of palaeo-coastal dune accumulations.

At Robberg aeolianite/dune accretion formation was confined to early and late MIS 3 and to the early Holocene, providing the first evidence for onshore MIS 3 aeolianite accumulation in the otherwise well-studied southern Cape aeolianite/coastal geomorphic record. This reflects: 1) the limited accommodation space of this headland environment (cf. embayments); 2) the character of the offshore topography;3) the hypothesised importance of an inherited offshore sediment supply source; in this case sediments reworked from the inner shelf and a putative spit-bar system formed in MIS 5e, analogous to that forming in the Holocene.

Moving beyond Robberg and the southern Cape, this study emphasises the necessity of having both on-shore and off-shore topographic and lithological data to consider sediment sources, transportation pathways and shoreline positions through time.

It also demonstrates challenges when scaling between site-scale studies to regional scale considerations and controls; in that local off-shore or on-shore contexts at times exert greater influence on the preserved aeolianite record than regional-scale trends in sea-level and climatic conditions. The distinct timing of dune accumulation in Hoffman's Cave illustrates the importance of this point in the context of the region's coastal archaeological record (**Figure S3**), and this observation is relevant to interpretations of the stratigraphic record at several coastal rock-shelter sites (see Carr et al. 2016, also Jacobs, 2010).

Acknowledgements

The University of Leicester funded ASC's field and laboratory work. Rob Ashurst assisted with the preparation of the OSL samples in Sheffield. Professor Andy Saunders is thanked for assistance with the ICP-MS measurements. Further support for fieldwork and radiocarbon dating came from the South African Research Chairs initiative of the National Research Foundation and the Department of Science and Technology of South Africa (grant no 84407) to JS. Sediment samples were collected in accordance with permit number 0052-AAA008-00011, issued by the Western Cape Nature Conservation Board. Two anonymous reviewers are thanked for their constructive comments.

References

Aitken, M.J 1985. Thermoluminescence Dating. Academic Press, 370p

Amante, C. and Eakins, B. (2009). ETOPO1 - 1 Arc-Minute Global Relief Model: Procedures, Data Sources and Analysis. NOAA Technical Memorandum NESDIS NGDC, 24, 19pp.

Andreucci, S., Clemmensen, L.B., Pascucci, V. 2010a. Transgressive dune formation along a cliffed coast at 75 ka in Sardinia, Western Mediterranean: a record of sea-level fall and increased windiness. Tera Nova 22, 424-433.

Andreucci, S., Clemmensen, L.B., Murray, A.S., Pascucci, V. 2010b. Middle to late Pleistocene coastal deposits of Alghero, northwest Sardinia (Italy): Chronology and evolution. Quaternary International 222, 3-16.

Andreucci, S., Bateman, M.D., Zucca, C., Kapur, S., Akşit, I., Dunajko, A. Pascucci, V. 2012. Evidence of Saharan dust in Upper Pleistocene reworked palaeosols of Northwest Sardinia, Italy: Palaeoenvironmental implications. Sedimentology 59, 917-938.

Bateman, M.D., Holmes, P.J., Carr, A.S., Horton, B.P., Jaiswal, M.K. 2004. Aeolianite and barrier dune construction spanning the last two glacial-interglacial cycles from the southern Cape coast, South Africa Quaternary Science Reviews 23, p1681-1698

Bateman, M.D., Carr, A.S., Murray-Wallace, C.V., Holmes, P.J., Roberts, D.L. 2008. A dating inter-comparison study on Late Stone Age Midden deposits, South Africa. Geoarchaeology, 23, 715-741

Bateman, M.D., Carr. A.S., Holmes, P.J., Dunajko, A., McLaren, S.J., Marker, M.E., Roberts, D.L, Murray-Wallace, C.V., Bryant, R.G. 2011. The evolution of barrier dune systems: A case study of the Middle-Late Pleistocene Wilderness barrier dunes, South Africa. Quaternary Science Reviews 30, 63-81

Bell, W.T. 1979. Thermoluminescence dating: radiation dose rate data. Archaeometry 21,243-246

Birch, G.F., 1978. Nearshore Quaternary Sedimentation off the South Coast of South Africa, Joint Geological Survey, University of Cape Town, Technical Report 11, 127-146.

Birch, G.F., De Plessis, A., Willis, J.P. 1978. Offshore and on land geological and geophysical investigations in the Wilderness Lakes region. Transactions of the Geological Society of South Africa 81, 339-352.

Botha, G.A., Bristow, C.S., Porat, N., Duller, G.A.T., Armitage, S.J., Roberts, H.S., Clarke, B.M., Kota, M.W., Schoeman, P. 2003. Evidence for dune reactivation from GPR profiles on the Maputaland coastal plain, South Africa. Geological Society of London, Special Publications 211, 29-46.

Bremner, J.M., 1983. Properties of logarithmic spiral beaches with particular reference to Algoa Bay. In: McLachlan, A., Erasmus, T. (Eds.) Sandy beaches as ecosystems. Junk: The Hague, 97-113.

Broad, D.S., Jungslager, E.H.A., McLachlan, I.R., Roux, J. 2006. Offshore Mesozoic Basins, In: The Geology of South Africa, Johnson MR, Anhaeusser C.R., Thomas RJ. (Eds). The Geological Society of South Africa and Council for Geoscience, Pretoria, p553-571

Brooke, B. 2001. The distribution of carbonate eolianite. Earth-Science Reviews 55, 135-164.

Brooke, B.P., Olley, J.M., Pietsch, T., Playford, P.E., Haines, P.W., Murray-Wallace, C.V., Woodroffe, C.D. 2014. Chronology of Quaternary coastal aeolianite deposition and the drowned shorelines of southwestern Western Australia–a reappraisal. Quaternary Science Reviews 93, 106-124.

Brooke, B.P., Nichol, S.L., Huang, Z., Beaman, R.J. 2017. Palaeoshorelines on the Australian continental shelf: Morphology, sea-level relationship and applications to environmental management and archaeology Continental Shelf Research 134, 26-38.

Brown Jr., L.F., Benson, J.M., Brink, G.J., Doherty, S., Jollands, A., Jungslager, E.H.A., Keenan, J.H.G., Muntingh, A., van Wyk, N.J.S., 1995. Sequence stratigraphy in offshore South African divergent basins: an atlas on exploration for cretaceous lowstand traps by Soekor (Pty) Ltd. AAPG Studies in Geology 41.

Butzer, K.W., Helgren, D.M. 1972. Late Cenozoic evolution of the cape coast between Knysna and Cape St. Francis, South Africa. Quaternary Research 2, 143-169

Carr, A.S. Thomas, D.S.G., Bateman, M.D. 2006. Climatic and sea-level controls on Late Quaternary eolian activity on the Agulhas Plain, South Africa. Quaternary Research 65, 252-263

Carr, A.S., Bateman, M.D., Holmes, P.J. 2007. Developing a 150 ka luminescence chronology for the barrier dunes of the southern Cape, South Africa. Quaternary Geochronology 2, 110-116

Carr, A.S., Bateman, M.D., Roberts, D.L., Murray-Wallace, C.V., Jacobs, Z., Holmes, P.J. 2010. The last interglacial sea-level high stand on the southern Cape coastline of South Africa. Quaternary Research 73, 351-362

Carr, A.S., Chase. BM. Mackay, A. 2016. Mid to Late Quaternary Landscape and Environmental Dynamics in the Middle Stone Age of Southern South Africa. In: Jones, S., Stewart, B.A., (Eds.), Africa from MIS 6-2: Population Dynamics and Paleoenvironments. Springer, Dordrech, 23-47.

Cawthra, H.C., Uken, R., Oveckhina, M., 2012. New insights into the geological evolution of the Bluff Ridge and adjacent Blood Reef, Durban, South Africa. South African Journal of Geology 115, 291-308.

Cawthra, H.C., Bateman, M.D., Carr, A.S., Compton, J.S., Holmes, P.J. 2014. Understanding Late Quaternary change at the land–ocean interface: a synthesis of the evolution of the Wilderness coastline, South Africa. Quaternary Science Reviews 99, 210-223.

Cawthra, H.C., Compton, J. S., Fisher, E. C., MacHutchon, M.R., Marean, C. W., 2015. Submerged terrestrial landscape features off the South African south coast. In: Harff, J., Bailey, G., Lüth F. (Eds.) Geology and Archaeology: Submerged landscapes of the continental shelf. Special Publication of the Geological Society of London 411, 219-233.

Cawthra, H.C., Jacobs, Z., Compton, J.S., Fisher, E.C., Karkanas, P., Marean, C.W. 2018. Depositional and sea-level history from MIS 6 (Termination II) to MIS3 on the southern continental shelf of South Africa. Quaternary Science Reviews 181, 156-172.

Compton, J.S. 2001. Holocene sea-level fluctuations inferred from the evolution of depositional environments of the southern Langebaan Lagoon salt marsh, South Africa. The Holocene 11, 395–405.

Cooper, J.A.G. 2001. Geomorphological variability among microtidal estuaries from the wave-dominated South African coast. Geomorphology 40, 99-122.

Claassen, D. 2014. Geographical controls on sediment accretion of the Cenozoic Algoa group between Oyster Bay and St. Francis, eastern cape coastline, South Africa. South African Journal of Geology, 117, 109-128.

Clemmensen, L.B., Fornós, J.J., Rodriguez-Perea, A. 1997. Morphology and architecture of a late Pleistocene cliff-front dune, Mallorca, Western Mediterranean. Terra Nova 9, 251-254

Deacon, J. 1984. The Later Stone Age of southernmost Africa. Oxford: British Archaeological Reports International Series 213.

De Decker, R.H., 1983. The Sediments of Plettenberg Bay and the Submerged Robberg Spit. Joint Geological Survey/ University of Cape Town Technical Report, 14: 255 - 265.

de Wet, W. 2013. Bathymetry of the South African continental shelf. Unpublished MSc thesis, University of Cape Town.

Dingle, R.V., Rogers, J. 1972. Pleistocene palaeogeography of the Agulhas Bank. Transactions of the Royal Society of South Africa, 40, 155-165.

Duller, G.A.T. 2003. Distinguishing quartz and feldspar in single grain luminescence measurements. Radiation Measurements 37, 161-165

Dunajko, A.C., Bateman, M.D. 2010. Sediment provenance of the Wilderness barrier dunes, southern Cape coast, South Africa. Terra Nova 22, 417-423

Fornós, J.J., Clemmensen, L.B., Gómez-Pujol, L., Murray, A.S. 2009. Late Pleistocene carbonate aeolianites on Mallorca, Western Mediterranean: a luminescence chronology. Quaternary Science Reviews 28, 2697-2709.

Flemming, B.W., Eagle, G.A., Fricke, A.H., Hunter, I.T., Martin, A.K., Schumann, E.H., Swart, V.P., Zoutendyk, P. 1983. Agulhas Bank Studies Report 11, Stellenbosch National Research Institute for Oceanology Memo 8319, 78 pp.

Galbraith, R.F., Roberts, R.G., Laslett, G.M., Yoshida H., Olley, J.M. 1999. Optical dating of single and multiple grains of quartz from Jinmium rock shelter, northern Australia, part 1, Experimental design and statistical models. Archaeometry 41, 339-364

Guérin, G., Mercier, N., Adamiec, G. 2011. Dose-rate conversion factors: update. Ancient TL 29, 5-8.

Hellström G.B., Lubke R. A. 1993. Recent Changes to a Climbing-Falling Dune System on the Robberg Peninsula Southern Cape Coast, South Africa. Journal of Coastal Research 9, 647-653

Heydorn, A.E.F., Tinley, K.L., 1980. Estuaries of the Cape part 1: Synopsis of the Cape coast, natural features, dynamics and utilisation. CSIR Research Report 380.

Illenberger WK. 1996. The geomorphic evolution of the Wilderness dune cordons, South Africa. Quaternary International, 33: 11–20.

Illenberger, W.K., Burkinshaw, J.R. 2008. Coastal dunes and dunefields. In: Geomorphology of the Eastern Cape, Lewis CA (Ed). NICS, Grahamstown, p85-106.

Inskeep, R.R. 1987. Nelson Bay Cave, Cape Province, South Africa: the Holocene levels. Oxford: British Archaeological Reports International Series 357.

Jacobs, Z., Wintle, A.G., Duller, G.A.T. 2003. Optical dating of dune sand from Blombos Cave, South Africa: I—multiple grain data. Journal of Human Evolution, 44, 599–612.

Jacobs, Z., Duller, G.A.T., Wintle, A.G. 2003. Optical dating of dune sand from Blombos Cave, South Africa: II—single grain data. Journal of Human Evolution 44, 613-625.

Jacobs, Z. 2010. An OSL chronology for the sedimentary deposits from Pinnacle Point Cave 13B - a punctuated presence. Journal of Human Evolution 59, 289-305.

Kim G., Yang H.-S., Church T.M. 1999. Geochemistry of alkaline earth elements (Mg, Ca, Sr, Ba) in the surface sediments of the Yellow Sea. Chemical Geology 153, 1-10.

Klein, R.G. 1972 Preliminary report on the July through September 1970 excavations at Nelson Bay Cave, Plettenberg Bay (Cape Province, South Africa). Palaeoecology of Africa 6, 177-208.

Kyriacou, K. 2009. The reinvestigation of Hoffman's/Robberg Cave – the artefactual and shellfish assemblages, 2007. Unpublished MPhil thesis, University of Cape Town.

Lisiecki, L.E., Raymo, M.E. 2005. A Pliocene-Pleistocene stack of 57 globally distributed benthic δ18O records. Paleoceanography 20 (1)

Marker, M.E., Miller, D.E. 1993. A mid-Holocene high stand of the sea at Knysna. South African Journal of Science 89, 106-107.

Marker, M.E., Holmes, P.J. 2010. The geomorphology of the Coastal Platform in the southern Cape. South African Geographical Journal 92, 105-116

Martin, A.R.H. 1962. Evidence relating to the Quaternary history of the Wilderness lakes. Transactions of the Geological Society of South Africa, 65 19-45.

Martin, A.K., Hartnady, C.J.H. 1986. Plate tectonic development of the southeast Indian Ocean: A revised reconstruction of East Antarctica and Africa, Journal of Geophyiscal Research, 91, 4767-4786.

Martin, A.K., Flemming, B.W. 1986. The Holocene shelf sediment wedge off the south and east coast of South Africa. In Shelf sands and sandstones. Knight RJ, McLean JR. (Eds). Canadian journal of Petroleum Geologists Memoir 11, 27-44.

Mejdahl, V. 1979 Thermoluminescence dating – beta-dose attenuation in quartz grains. Archaeometry 21, 61-72.

Murray, A.S., Wintle A.G., 2000. Luminescence dating of quartz using an improved single-aliquot regenerative-dose protocol. Radiation Measurements 32, 57-73.

Murray, A.S., Wintle, A.G 2003. The single-aliquot regenerative-dose protocol: potential for improvements in reliability. Radiation Measurements 37, 377-381.

Newton, A.R., Shone, R.W., Booth, P.W.K. 2006. The Cape Fold Belt. In: Johnson, M.R., Anhaeusser, C.R., Thomas, R.J. (Eds.) The Geology of South Africa, Geological Society of South Africa, Council for Geoscience Pretoria, 521-531, 2006.

Porat, N., Botha, G.A. 2008. The luminescence chronology of dune development on the Maputaland coastal plain, southeast Africa. Quaternary Science Reviews 27, 1024-1046.

Prescott, J.R., Hutton, J.T. 1994. Cosmic ray contributions to dose rates for luminescence and ESR dating: large depths and long-term variations. Radiation Measurements 23, 497-500.

Reddering, J.S.V., 1983. An inlet sequence produced by migration of a small microtidal inlet against longshore drift: the Keurbooms Inlet, South Africa. Sedimentology 30, 201-218.

Reddering, J.S.V. 1988. Evidence for a Middle Holocene transgression, Keurbooms estuary, South Africa. Palaeoecology of Africa 19, 79-86.

Reddering, J.S.V. 2003. Lithostratigraphy of the Robberg Formation (Uitenhage Group), including the St. Sebastian Point Member. South African Committee for Stratigraphy, Lithostratigraphic Series 40, Council for Geoscience 20 pp.

Roberts, D., Murray-Wallace, C.V., Bateman, M.D., Carr, A.S., Holmes, P.J. 2008. Fossil elephant trackways, sedimentation and diagenesis in OSL/AAR-dated Late Quaternary coastal aeolianites: Still Bay, South Africa. Palaeogeography Palaeoclimatology Palaeoecology 257, 261-279

Roberts, D., Murray-Wallace, C.V., Bateman, M.D., Carr, A.S., Holmes, P.J. 2009. West coast dune plumes: climate driven contrasts in dunefield morphogenesis along the western and southern South African Coasts. Palaeogeography Palaeoclimatology Palaeoecology 271, 34-48.

Roberts, D.L., Karkanas, P., Jacobs, Z., Marean, C.W., Roberts, R.G. 2012. Melting ice sheets 400,000 yr ago raised sea level by 13 m: Past analogue for future trends Earth and Planetary Science Letters 357, 226-237.

Roberts, D.L., Cawthra, H., Musekiwa, C. 2013. Dynamics of late Cenozoic aeolian deposition along the South African coast: a record of evolving climate and ecosystems. Geological Society, London, Special Publications 388, 353-387

Rogers, J., 1971. Sedimentology of Quaternary deposits on the Agulhas Bank. Bulletin of the South African National Committee for Oceanography, 1, 117 pp.

Rudner, J., Rudner, I. 1973. A note on early excavations at Robberg. South African Archaeological Bulletin 28, 94-96.

Sanderson, P.G., Eliot, I. 1996. Shoreline salients, cuspate forelands and tombolos on the coast of Western Australia. Journal of Coastal Research, 761-773.

South African Navy Hydrographic Office (SANHO), 1972. SAN Chart 1022 Plettenbergbaai, 1 pp.

Shaw, A.E., Holmes, P.J., Rogers, J. 2001. Depositional landforms and environmental change in the headward vicinity of Dias Beach, Cape Point. South African Journal of Geology 104, 101–114.

Shone, R.S. 2006. Onshore post-Karoo Mesozoic deposits. In: Johnson, M.R., Anhaeusser, C.R., Thomas, R.J. (Eds.). The Geology of South Africa. Geological Society of South Africa, Council for Geoscience, Pretoria, 541–552.

Silvester, R., 1974. Developments in geotechnical engineering 4B. Coastal Engineering II. Sedimentation, estuaries, tides, effluents and modelling. Elesvier, Amsterdam.

Taylor, S.R. McLennan, S.M. 1985. The continental crust: its composition and evolution. Oxford: Blackwell Scientific

Thomsen, K.J., Murray, A.S., Buylaert, J.P., Jain, M., Hansen, J.H., Aubry, T. 2016. Testing single-grain quartz OSL methods using sediment samples with independent age control from the Bordes-Fitte rockshelter (Roches d'Abilly site, Central France). Quaternary Geochronology 31, 77-96

Tinker, J.H., de Wit, M.J., Brown R.W. 2008a Mesozoic exhumation of the southern Cape, South Africa, quantified using apatite fission track thermochronology. Tectonophysics, 455, 77–93.

Tinker, J.H., de Wit, M.J., Brown R.W. 2008b. Linking source and sink: evaluating the balance between onshore erosion and offshore sediment accumulation since Gondwana break-up, South Africa. Tectonophysics 455, 94–103.

Tinley, K.L. 1985. Coastal Dunes of South Africa. South African National Scientific Programmes Report No. 109, Foundation for Research Development, Council for Scientific and Industrial Research, Pretoria, 300 pp.

Toerien, D.K., 1979. Die geologie van die gebied Oudtshoorn. Toeligting van blad 3322, Skaal 1: 250 000. Department van Mynwese, Geologiese Opname van Suid-Afrika, 34 pp.

Tripp, R.T., 1967. An atlas of coastal surface drifts: Cape Town to Durban. Report of the South African Oceanographic Data Centre, University of Cape Town.

del Valle, L., Gomez-Pujol, L., Fornos, J.J., Timar-Gabor, A., Anechiteie-Deacu V., Pomar, F. 2016. Middle to Late Pleistocene dunefields in rocky coast settings at Cala Xuclar (Eivissa, Western Mediterranean): Recognition, architecture and luminescence chronology. Quaternary International 407, 4-13

Waelbroeck, C., Labeyrie, L., Michel, E., Duplessy, J.C., McManus, J.F., Lambeck, K., Balbon, E., Labracherie, M. 2002. Sea-level and deep water temperature changes derived from benthonic foraminifera isotopic records. Quaternary Science Reviews, 21 295–305.

Whitfield AK, Allanson BR, Heinecken TJE. 1983. Report 22 of the Estuaries of the Cape, Part 2: Synopses of available information on individual systems, edited by Heydorn AEF and Grindley, JR. Stellenbosch: CSIR. (CSIR research report 421), CSIR Research Report number 421.

Figures

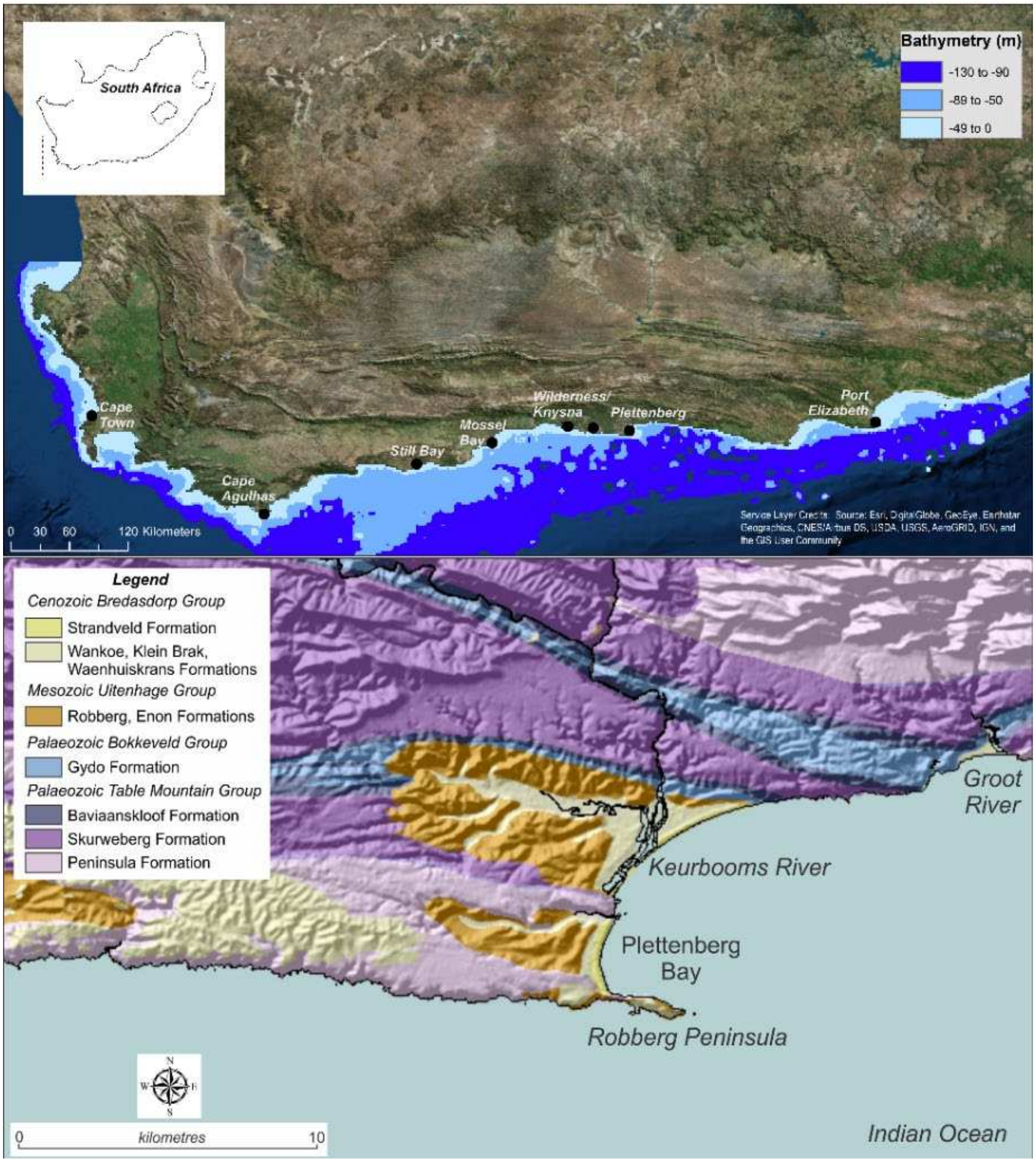

Service Layer Credits: Source: Esri, DigitalGlobe, GeoEye, Earthstar Geographics, CNES/Airbus DS, USDA, USGS, AeroGRID, IGN, and the GIS User Community

Figure 1: *Upper panel – the location of Plettenberg Bay and other locales mentioned in the text. The continental shelf bathymetry was derived from the ETOPO1 data (Amante and Eakins, 2009) and have been shaded by depth in segments relevant to the later discussion (note in particular the varied distance*

of the -50 m isobath from the shoreline). Lower panel – the geology of the Robberg Peninsula and Plettenberg Bay study area.

Figure 2: *The Robberg Peninsula, with the sample sites and other locales mentioned in the text marked.*

***Figure 3**: Aeolianite sampling sites on the southeast margin of the Robberg Peninsula. A) Sampling location for Leic13004 – the contrasting dip of the aeolianite outcrops in the right and centre of the images contrasts with the Robberg Formation outcrops to the left. The edge of the contemporary shore platform is visible in the lower left. B) Leic13005 – steeply dipping aeolianites (left) unconformably overlie and sit within the topography of the Robberg Formation (right and lower left).*

***Figure 4**: Panoramic view of The Island looking to the east from the western shoreline (immediately above Leic13001). The upper palaeosol "P2" is marked and follows the topography of the modern Island surface. The sample location for Leic13002, which overlies P2 (see also **Figure 9d)** is shown to the left with a large*

shell midden immediately stratigraphically overlying the OSL sample, from which a radiocarbon date from a Perna perna *shell was obtained (**Table S1**).*

***Figure 5**: A) view northwards of the tombolo from The Island. The narrow area of active sands that forms Witsand climbing dune system extends from the large apron of bare sand on the middle right of figure 5a. B) View of the cliff front echo dune (sampling site is slightly left of centre on the dune crest-line C) view of the island and tombolo from the west. D) view of the mouth of Hoffman's Cave.*

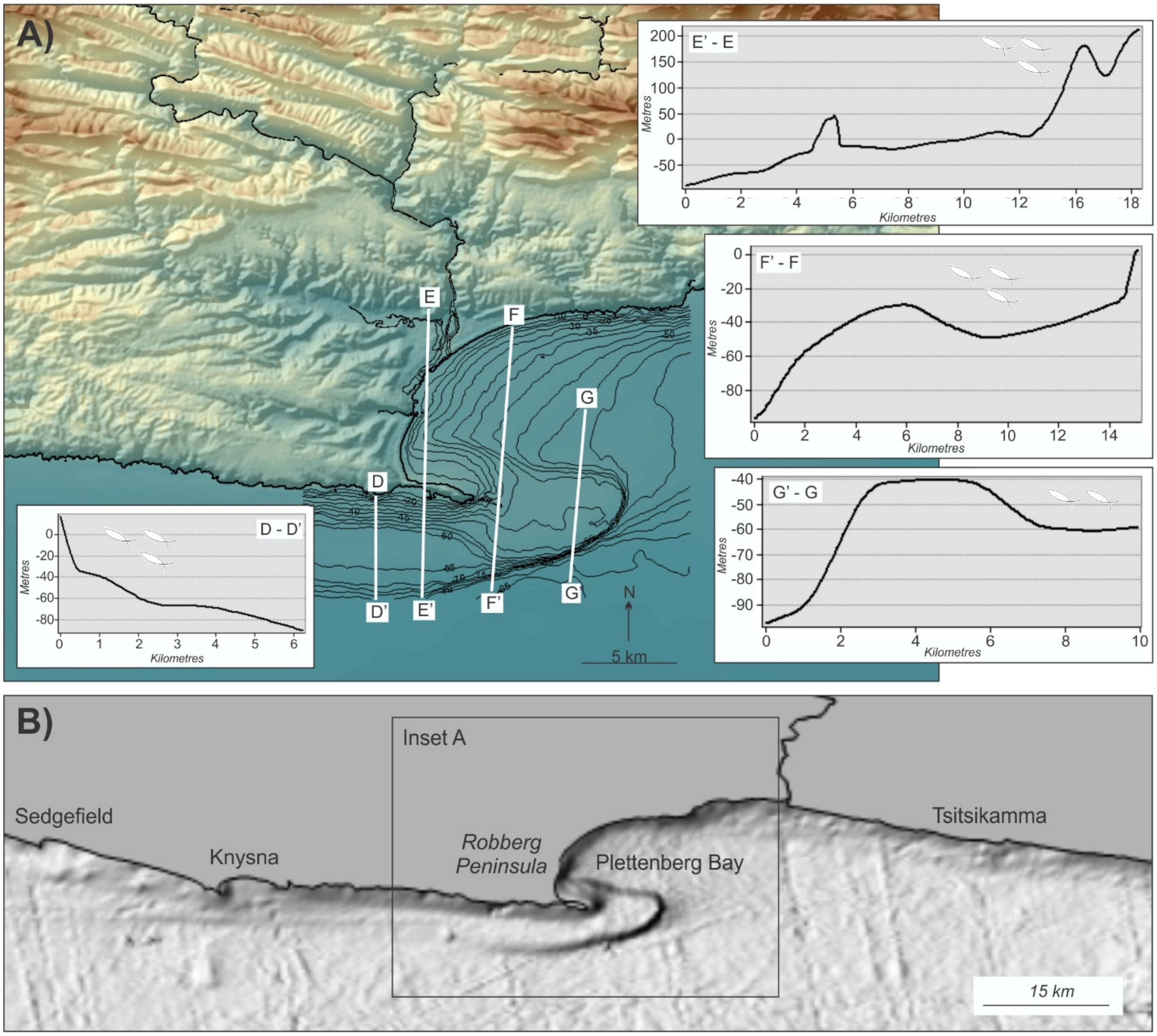

Figure 6 *Bathymetry around the Robberg Peninsula – profiles F and G highlight the submerged spit bar feature south of Plettenberg Bay.*

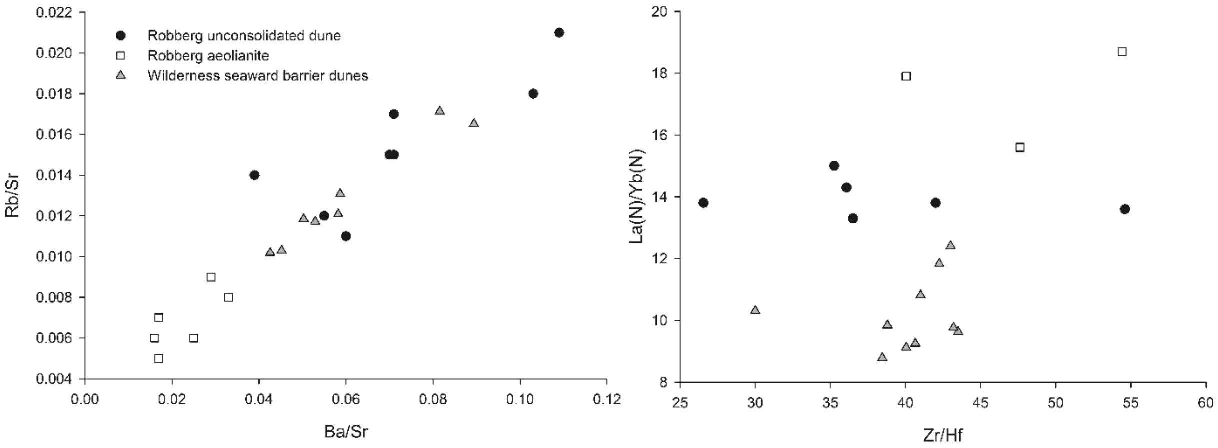

Figure 7: *Selected elemental ratios for the Robberg dune sands and aeolianites, with data from the Wilderness Embayment for comparison. Left: Element ratios generally associated with immobile elements (the La and Yb data are normalised to chondrite values: Taylor and McLennan (1985)). Right: Ca-associated alkali earth elements ratios for Robberg dunes, Robberg aeolianite and the Wilderness seaward barrier.*

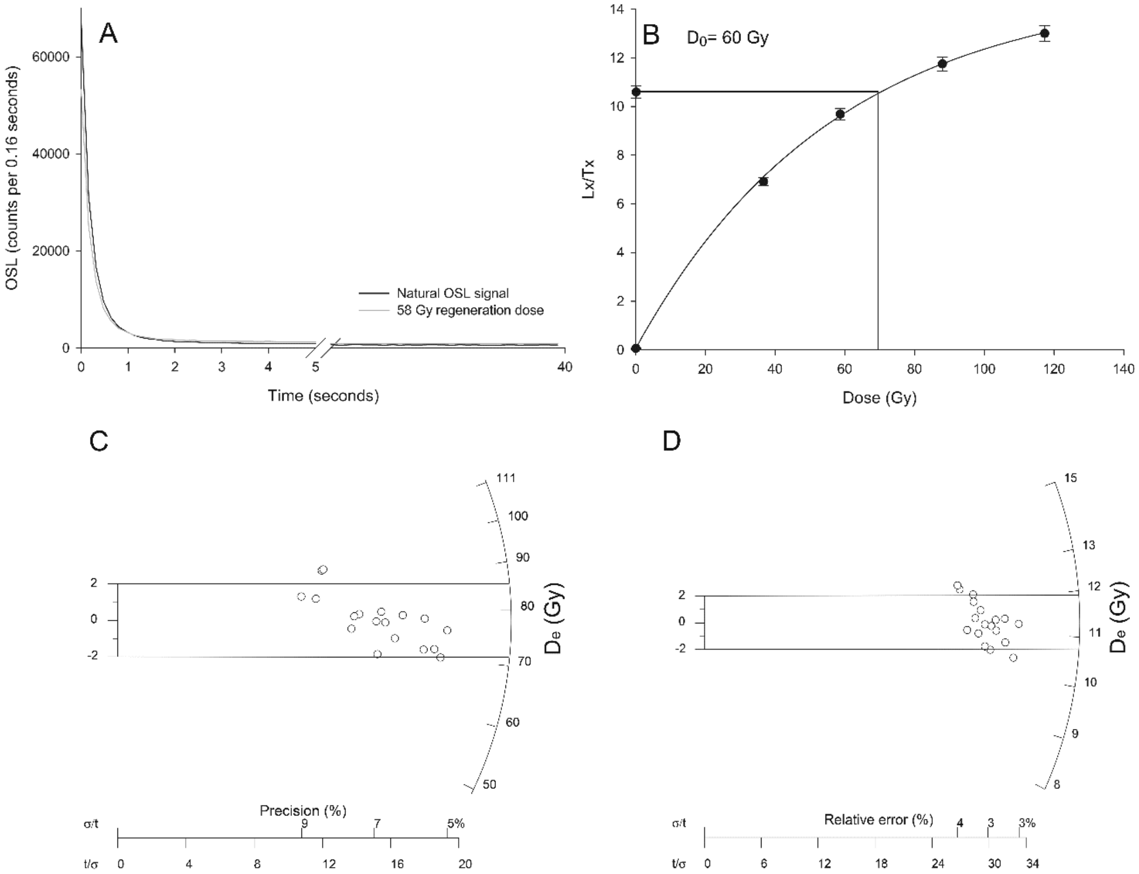

Figure 8*: Example OSL shine down (A) and dose-response curve (B) from Leic13001. Two radial plots (C: Leic13001 and D: Leic13002) illustrate the inter-aliquot scatter in single aliquot (9 mm aliquots) equivalent dose distributions . Note that all data points falling with the two horizontal bars can be considered statistically (within 2 sigma) identical.*

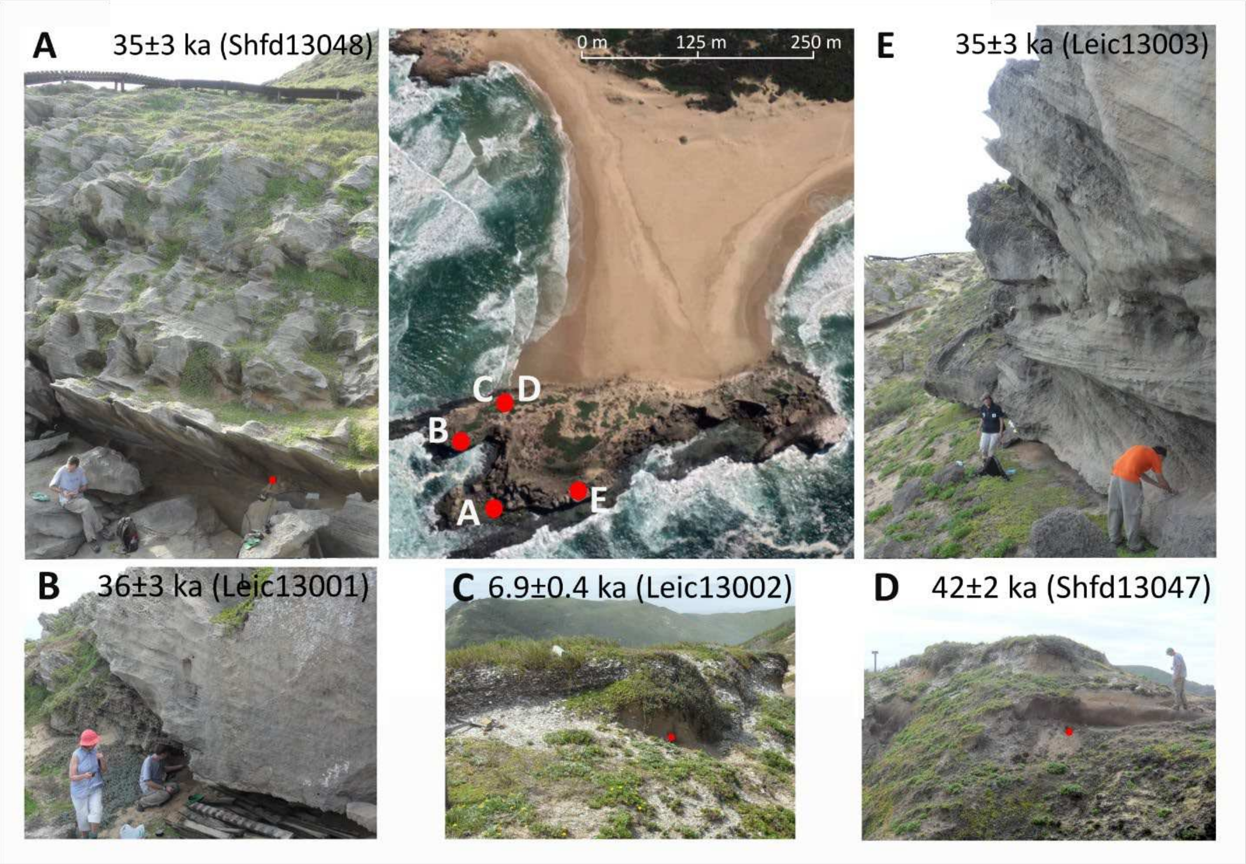

***Figure 9**: Summary of site ages and sampling locations from The Island. Leic13003 (E) immediately overlies P1.*

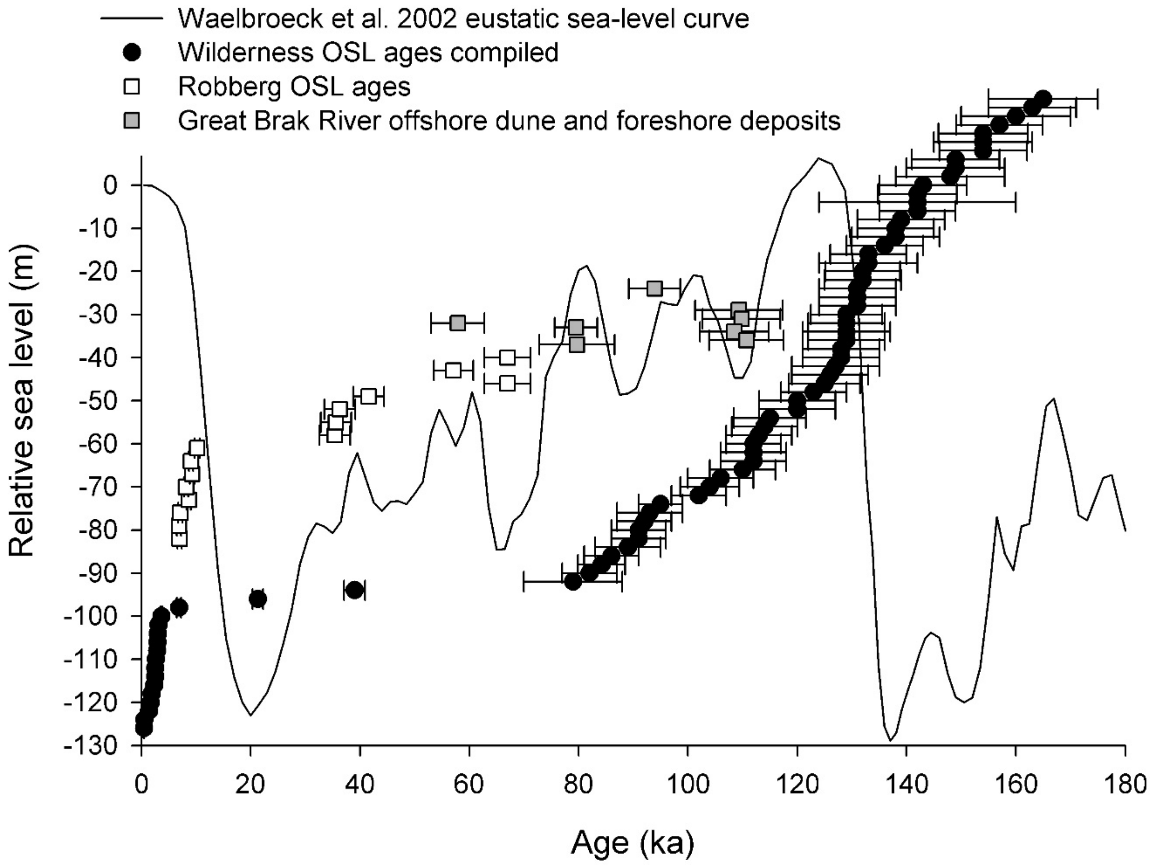

Figure 10: *Comparison of OSL ages for dunes and aeolianite of the Wilderness Embayment (filled circles; Bateman et al., 2011), the Great Brak River offshore dune and foreshore deposit OSL ages (Grey squares; Cawthra et al. 2018) and the new Robberg Peninsula dune ages (open squares). Note that the OSL ages are plotted with arbitrary y axis values.*

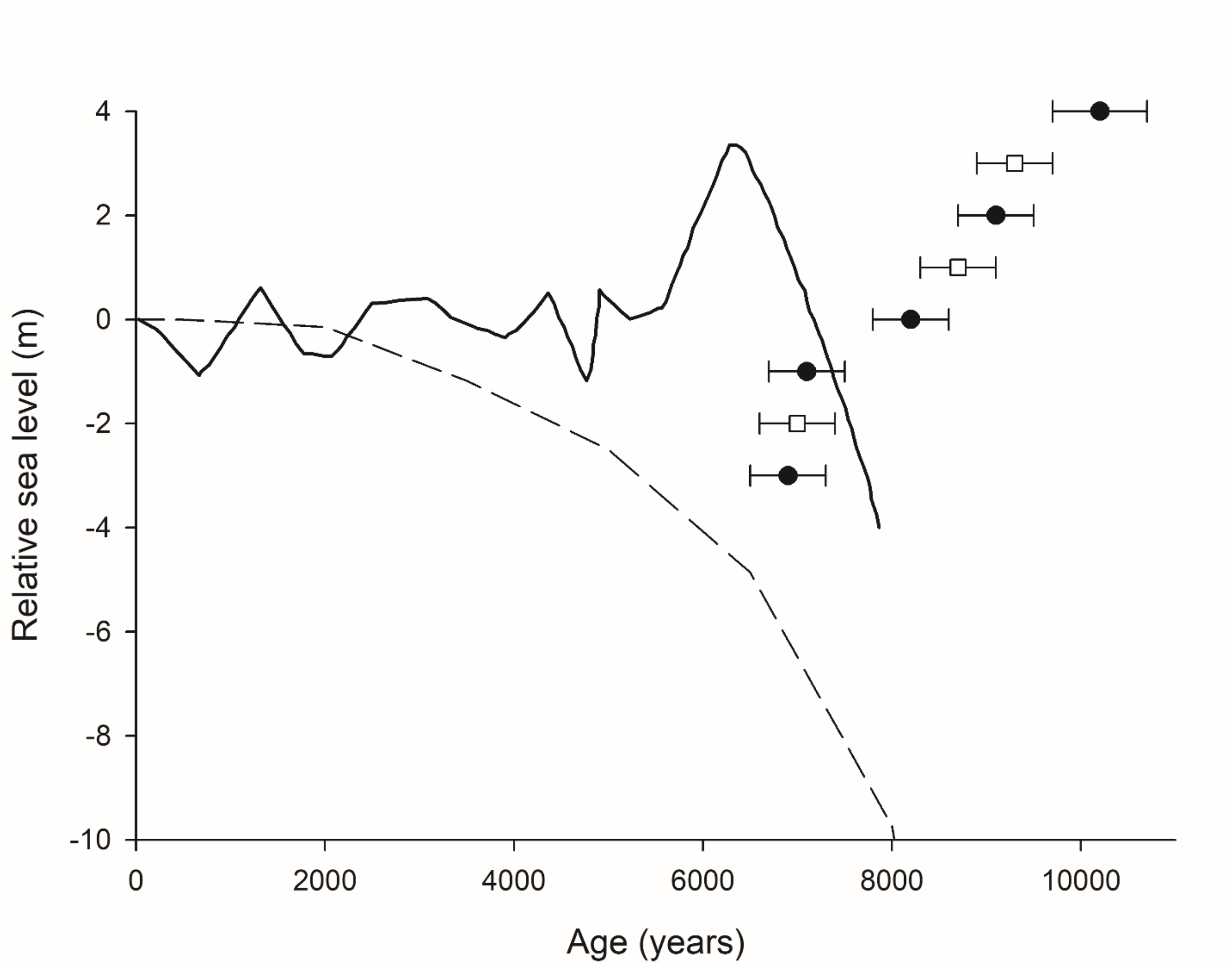

Figure 11: *Holocene dune ages in relation to the Holocene RSL curve of Compton (2001) (Solid line) and Waelbroeck et al 2002) (dashed line). Filled circles = coastal dunes (echo dune and dune sample from The Island, open squares = dune sands within Hoffman's Cave*

Tables

Field Code	Lab Code	Depth (m)	Location	N/N_m	Aliquot size	CAM D_e (Gy)	OD (%)	Average ratio to D_0*	Total Dose rate (Gy ka^{-1})	Age (ka)
ROB13-1-2	Leic13002	1.3	The Island	18/18	9 mm	11.3 ± 0.36	3	nd	1.62 ± 0.08	**6.9 ± 0.4**
ROB13-1-2			The Island	17/18	2 mm	10.7 ± 0.47	11	nd	1.62 ± 0.08	**6.6 ± 0.4**
ROB13-1-1	Leic13001	3.1	The Island	18/22	9 mm	77.7 ± 2.82	5	1.6 ± 0.4	2.18 ± 0.15	**35.6 ± 2.8**
ROB13-1-3	Shfd13047	3.0	The Island	20/24	9 mm	77.7 ± 1.66	16	nd	1.87 ± 0.12	**41.6 ± 2.8**
ROB13-2-1	Shfd13048	12.25	The Island	20/24	9 mm	59.5 ± 1.84	28	nd	1.68 ± 0.12	**35.4 ± 2.8**
ROB13-2-2	Leic13003	6.5	The Island	18/23	9 mm	80.2 ± 3.75	12	2.0 ± 0.6	2.31 ± 0.16	**34.7 ± 2.9**
ROB13-3-1	Leic13004	10	Peninsula	20/20	9 mm	58.6 ± 2.37	11	1.3 ± 0.2	0.88 ± 0.04	**67.0 ± 4.2**
ROB13-3-2	Shfd13049	11.2	Peninsula	17/23	9 mm	55.0 ± 0.77	15	nd	0.96 ± 0.06	**57.1 ± 3.6**
ROB13-3-3	Leic13005	12	Peninsula	22/25	2 mm	57.7 ± 2.06	6	1.7 ± 0.4	1.04 ± 0.06	**55.5 ± 3.7**
HRC13-2-4	Leic13008	3.3	Echo dune	22/22	9 mm	4.71 ± 0.16	7	nd	0.57 ± 0.02	**8.2 ± 0.4**
HRC13-2-4				25/25	2 mm	4.25 ± 0.15	8	nd	0.57 ± 0.02	**7.4 ± 0.4**
HRC13-2-4				43/900	Single grain	4.46 ± 0.30	32	nd	0.57 ± 0.02	**7.8 ± 0.6**
HRC13-2-1	Leic13007	6.8	Echo dune	21/21	9 mm	4.94 ± 0.16	4	nd	0.69 ± 0.04	**7.1 ± 0.4**
HRC13-2-1				25/25	2 mm	4.68 ± 0.18	11	nd	0.69 ± 0.04	**6.8 ± 0.4**
HRC13-2-1				38/1400	Single grain	4.87 ± 0.26	17	nd	0.69 ± 0.04	**7.0 ± 0.5**
HRC13-2-2	Shfd13052	8.8	Echo dune	22/24	9 mm	6.66 ± 0.07	6	nd	0.73 ± 0.03	**9.1 ± 0.4**
HRC13-2-3	Shfd13053	9.8	Echo dune	20/24	9 mm	8.04 ± 0.10	8	nd	0.79 ± 0.04	**10.2 ± 0.5**
HRC13-1-1	Leic13006	3.3	Hoffman’s Cave	28/28	9 mm	3.84 ± 0.12	5	nd	0.54 ± 0.03	**7.0 ± 0.3**
HRC13-1-2	Shfd13050	4.6	Hoffman’s Cave	22/23	9 mm	4.55 ± 0.05	6	nd	0.53 ± 0.02	**8.7 ± 0.4**
HRC13-1-3	Shfd13051	5.5	Hoffman’s Cave	19/24	9 mm	4.80 ± 0.04	6	nd	0.53 ± 0.02	**9.3± 0.4**

* for all measured aliquots – includes aliquots rejected for D_0 ratio >2

Note: for single grain measurements the “intrinsic” OD obtained measuring gamma irradiated quartz is 9%

Table 2: Particle size distribution data for the dunes and aeolianite of the Robberg Peninsula

	Mean (Phi)	**Median (Phi)**	**Sorting (Phi)**	**Skew**	**Kurtosis**
Aeolianites					
Leic13001	1.50	1.48	0.68	-0.06	0.99
Leic13003	1.62	1.62	0.63	-0.01	0.95
Leic13004	1.57	1.56	0.99	-0.20	1.56
Leic13005	1.89	1.87	0.68	-0.11	1.13
Dune sediments					
Leic13006	2.02	2.02	0.42	0.00	0.96
Leic13007	2.00	2.00	0.44	-0.02	0.94
Leic13008	1.86	1.86	0.41	0.00	0.96
Leic13002	2.23	2.18	0.98	-0.28	1.56